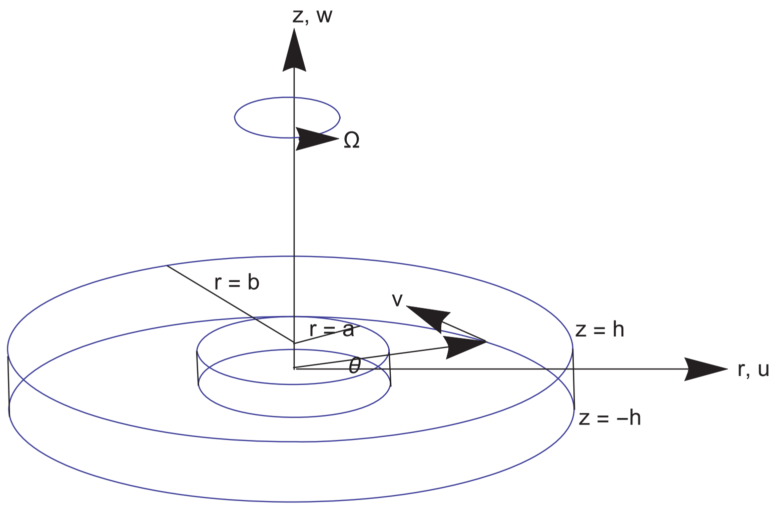

Source: Author's own work

Figure 1. Flow between narrow disks co-rotating at angular velocity Ω about the axial axis z

narrow gap between the disks. The disks are separate at a distance of $2h$ and possess inner and outer radii as a and b, respectively. The physical problem is such that the fluid entrance is allowed from the inner cylinder at $r = a$ and the flowing fluid is let to exit at the outer cylinder $r = b$. The axisymmetric flow motion and heat transfer in the cylindrical coordinates (r, θ, z) taking place in the rotating frame of reference are given by the subsequent governing equations:

$$
\begin{aligned}
\frac{1}{r}(ru)_r + w_z &= 0,\\
uu_r + wu_z - \frac{v^2}{r} - 2\Omega v &= -\frac{1}{\rho}p_r + \nu\left(u_{rr} + \frac{1}{r}u_r - \frac{u}{r^2} + u_{zz}\right),\\
uv_r + wv_z + \frac{uv}{r} + 2\Omega u &= \nu\left(v_{rr} + \frac{1}{r}v_r - \frac{v}{r^2} + v_{zz}\right),\\
uw_r + ww_z &= -\frac{1}{\rho}p_z + \nu\left(w_{rr} + \frac{1}{r}w_r + w_{zz}\right),\\
uT_r + wT_z &= \frac{k}{\rho c_p}\left(T_{rr} + \frac{1}{r}T_r + T_{zz}\right).
\end{aligned}
\tag{1}
$$

The terms multiplied by 2 on the left-hand side come from the Coriolis effects. Note that a few typographical errors in Batista (2011) can be witnessed while checking the relevant momentum equations. The flow field in equation (1) is equipped with the velocity vector (u, v, w) acting in the radial, circumferential and axial directions. The flow has constant fluid properties of density ρ, kinematic viscosity ν, thermal conductivity k and specific heat c_p. Moreover, p is the pressure and T is the temperature inside the gap region of the disks. It should be remarked that, due to the flow geometry adopted for the system (1), the circumferential velocity should be added the component Ωr and the pressure should be added the component $\frac{1}{2}\rho\Omega^2 r^2$ to get the total quantities in the inertial reference frame, as also stated in Batista (2011). The complementing boundary conditions are then given by:

$$
\begin{aligned}
&u(r,-h)=lu(r,-h)_z, \quad u(r,h)=-lu(r,h)_z,\\
&v(r,\pm h)=0, \quad w(r,\pm h)=0,\\
&T(r,\pm h)=\frac{c}{r},
\end{aligned}
\tag{2}
$$

where l is the slip factor in the radial direction, c is a wall temperature constant and the temperature boundary constraint offers a radially decaying temperature scenario from the inlet to outlet positions. This is in line with physical intuition such that the hot fluid entering into the tube (or rotor) exits the tube as cooled down.

As inferred from Batista (2011), it is adequate to introduce a constant flow rate at the tube exit $r=b$ to close the above equations in the manner:

$$
\frac{Q}{2\pi b}=\int_{-h}^{h}\left(u(r,z)|_{r=b}\right)dz. \tag{3}
$$

To make the system dimensionless, the following set is used Batista (2011):

$$
\begin{aligned}
&z=hz^*, \quad r=br^*,\\
&u=b\Omega u^*, \quad v=b\Omega v^*, \quad w=h\Omega w^*,\\
&p=\rho b^2\Omega^2 p^*, \quad T=\frac{c}{r}\Theta.
\end{aligned}
\tag{4}
$$

Substituting the set in (4) into equations (1)–(3), and further dropping the stars, we obtain the dimensionless set of equations:

$$
\begin{aligned}
&\frac{1}{r}(ru)_r+w_z=0,\\
&uu_r+wu_z-\frac{v^2}{r}-2v=-p_r+\frac{1}{\lambda^2}\left(\epsilon^2\left(u_{rr}+\frac{1}{r}u_r-\frac{u}{r^2}\right)+u_{zz}\right),\\
&uv_r+wv_z+\frac{uv}{r}+2u=\frac{1}{\lambda^2}\left(\epsilon^2\left(v_{rr}+\frac{1}{r}v_r-\frac{v}{r^2}\right)+v_{zz}\right),\\
&uw_r+ww_z=-\frac{1}{\epsilon^2}p_z+\frac{1}{\lambda^2}\left(\epsilon^2\left(w_{rr}+\frac{1}{r}w_r\right)+w_{zz}\right),\\
&u\left(-\frac{1}{r}\Theta+\Theta_r\right)+w\Theta_z=\frac{1}{Pr\lambda^2}\left(\epsilon^2\left(\Theta_{rr}-\frac{1}{r}\Theta_r+\frac{1}{r^2}\Theta\right)+\Theta_{zz}\right),\\
&u(r,-1)=Lu(r,-1)_z, \quad u(r,1)=-Lu(r,1)_z,\\
&v(r,\pm 1)=0, \quad w(r,\pm 1)=0,\\
&\Theta(r,\pm 1)=1.
\end{aligned}
\tag{5}
$$

In equation (5), we have the dimensionless gap ratio parameter:

$$
\epsilon=\frac{h}{b}, \tag{6}
$$

which is assumed to represent narrow gaps permitting the Navier's slip Navier (1823), the slip parameter:

$$
L=\frac{l}{h}, \tag{7}
$$

and the Reynolds number:

$$Re = \lambda^2 = h^2 \frac{\Omega}{\nu}. \tag{8}$$

Further describing a volume flow rate coefficient $C_w = \frac{Q}{b\nu}$ into equation (3), it turns out to be:

$$\frac{\epsilon C_w}{2\pi\lambda^2} = \int_{-1}^{1} u(1, z)dz. \tag{9}$$

It should be emphasized that the model given in equations (1) through (9) conforms exactly to that given in Batista (2011) in the absence of velocity slip and thermal field (except the typos found in Batista (2011)). Moreover, the experimental investigation in Schosser *et al.* (2019) shows that for the mass flow rate 12.6 and the Reynolds number 1402, the flow between two co-rotating disks is already turbulent. Also, the experiments in the latter and the analysis in Batista (2011) reveal laminar flow for Reynolds numbers less than 500. This is highly likely to be the range of validity of the steady-state approach. In addition, the specification of the temperature boundaries at the walls of the rotating disk as given by equation (2), with their dependence on the radial position is one of a special imposition, enabling us not to have to make further assumptions. Since r changes from inner ($a/b < 1$) to outer (1) locations, such a boundary constraint would imply physically that the hot fluid entering into the tube (or rotor) exits the tube as cooled down. On the other hand, if constant wall temperatures at the walls are imposed as in isothermal walls or if adiabatic conditions are applied, then further boundary conditions for temperature in the r-direction, i.e. the fluid entrance at $r = a$ and exit at $r = b$ have to be considered.

3. Series solutions

To obtain formal series solutions for equation (5) and further to gain insight into the limiting behavior, we expand the flow, pressure and temperature functions with the small perturbation parameter $\kappa = \frac{\epsilon}{r}$ [in compliance with the adoptions of Batista (2011) for the flow and pressure quantities] in the following forms:

$$\begin{aligned}
u &= \epsilon \sum_{n=0}^{\infty} \psi_n'(z)\kappa^{2n+1}, \\
v &= \epsilon \sum_{n=0}^{\infty} v_n(z)\kappa^{2n+1}, \\
w &= 2\sum_{n=0}^{\infty} (n+1)\psi_{n+1}(z)\kappa^{2n+4}, \\
p &= \epsilon^2 \left(p_0 \ln r + \sum_{n=0}^{\infty} p_{n+1}(z)\kappa^{2n+2} \right), \\
\Theta &= \sum_{n=0}^{\infty} \Theta_n(z)\kappa^{2n}.
\end{aligned} \tag{10}$$

We note that $\psi_n(z)$ in equation (10) is due to the stream function definition in cylindrical coordinate system ($u = r^{-1}\psi_z$, $w = -r^{-1}\psi_r$), and p_0 is a constant pressure to be determined.

A typo regarding w expansion also exists in Batista (2011). On substitution of equation (10) into equations (5) and (9), we get the leading and first-order system of differential equations:

$$
\begin{aligned}
v_0''(z) &= 2\lambda^2\psi_0'(z),\\
\psi_0'''(z) &= \lambda^2\left(p_0 - 2v_0(z)\right),\\
v_1''(z) &= 2\lambda^2\psi_1'(z),\\
\psi_1'''(z) &= -\lambda^2\left(2p_1(z) + 2v_1(z) + \psi_0'^2(z) + v_0^2(z)\right),\\
p_1'(z) &= 0,\\
\Theta_0''(z) &= 0,\\
\Theta_1''(z) &= -\left(1 + Pr\lambda^2\psi_0'(z)\right)\Theta_0(z),
\end{aligned}
\tag{11}
$$

complemented with the boundary conditions:

$$
\begin{aligned}
\psi_0'(-1) &= L\psi_0''(-1),\\
\psi_0'(1) &= -L\psi_0''(1),\\
v_0(\pm 1) &= 0,\\
\psi_0(1) - \psi_0(-1) &= \frac{C_w}{2\pi\epsilon\lambda^2},\\
\Theta_0(\pm 1) &= 1,\\
\psi_1(\pm 1) &= 0,\\
\psi_1'(-1) &= L\psi_1''(-1),\\
\psi_1'(1) &= -L\psi_1''(1),\\
v_1(\pm 1) &= 0,\\
\Theta_1(\pm 1) &= 0.
\end{aligned}
\tag{12}
$$

The higher order terms ($n \geq 0$) satisfy:

$$
\begin{aligned}
v_{n+2}''(z) &= -4(n+2)(n+1)v_{n+1}(z) + 2\lambda^2\psi_{n+2}'(z)\\
&\quad + \lambda^2\sum_{k=1}^{n+1}2k\left(\psi_k(z)v_{n+1-k}'(z) - v_k(z)\psi_{n+1-k}'(z)\right),\\
\psi_{n+2}'''(z) &= -4(n+2)(n+1)\psi_{n+1}'(z) - 2\lambda^2\left((n+2)p_{n+2}(z) + v_{n+2}(z)\right)\\
&\quad - \lambda^2\sum_{k=0}^{n+1}\left((2k+1)\psi_k'(z)\psi_{n+1-k}'(z) - 2k\psi_k(z)\psi_{n+1-k}''(z) + v_k(z)v_{n+1-k}(z)\right),\\
p_{n+2}'(z) &= \frac{2}{\lambda^2}(n+1)\left(4n(n+1)\psi_n(z) + \psi_{n+1}''(z)\right) - 4\sum_{k=1}^{n}k(n-1-2k)\psi_k(z)\psi_{n-k}'(z),\\
\Theta_{n+2}''(z) &= -(1 + 4(n+1)(n+2))\Theta_{n+1}(z) - Pr\lambda^2(1 + 2(n+1))\Theta_{n+1}(z)\psi_0'(z)\\
&\quad - Pr\lambda^2\sum_{k=0}^{n}\left((1+2k)\Theta_k(z)\psi_{n+1-k}'(z) - 2(1+k)\psi_{k+1}(z)\Theta_{n-k}'(z)\right),\\
&\quad (n \geq 0),
\end{aligned}
\tag{13}
$$

complemented with the boundary conditions:

$$\begin{aligned} \psi_{n+2}(\pm 1) &= 0, \\ v_{n+2}(\pm 1) &= 0, \\ \psi'_{n+2}(-1) &= L\psi''_{n+2}(-1), \\ \psi'_{n+2}(1) &= -L\psi''_{n+2}(1), \\ \Theta_{n+2}(\pm 1) &= 0, \\ (n &\geq 0). \end{aligned} \tag{14}$$

As a result, the task is next to evaluate the above system of differential equations consecutively with the input parameters ϵ, λ, C_w and L. Having solved the boundary-value problems in equations (11)–(12), the leading-order solutions [matching exactly with those in Breiter and Pohlhausen (1962) and Batista (2011) in the case of no-slip flow conditions] are found as:

$$\begin{aligned} \psi_0(z) &= c_{0,0} + c_{0,1}\cosh\lambda z\sin\lambda z + c_{0,2}\sinh\lambda z\cos\lambda z + c_{0,3}\cosh\lambda z\cos\lambda z + c_{0,4}\sinh\lambda z\sin\lambda z, \\ p_0 &= \frac{C_w(\cos 2\lambda + \cosh 2\lambda + L\lambda(-\sin 2\lambda + \sinh 2\lambda))}{\pi\epsilon\lambda(2L\lambda(\cos 2\lambda - \cosh 2\lambda) + \sin 2\lambda - \sinh 2\lambda)}, \\ v_0(z) &= \frac{\lambda^2 p_0 - \psi'''_0(z)}{2\lambda^2}, \\ \Theta_0(z) &= 1, \end{aligned} \tag{15}$$

where:

$$\begin{aligned} c_{0,1} &= -\frac{(\cosh\lambda(-\cos\lambda + 2L\lambda\sin\lambda) + \sin\lambda\sinh\lambda)p_0}{2\lambda(\cos 2\lambda + \cosh 2\lambda + L\lambda(-\sin 2\lambda + \sinh 2\lambda))}, \\ c_{0,2} &= -\frac{(\cos\lambda\cosh\lambda + (2L\lambda\cos\lambda + \sin\lambda)\sinh\lambda)p_0}{2\lambda(\cos 2\lambda + \cosh 2\lambda + L\lambda(-\sin 2\lambda + \sinh 2\lambda))}, \\ c_{0,3} &= 0, \\ c_{0,4} &= 0, \end{aligned} \tag{16}$$

followed by the first-order solutions:

$$\begin{aligned} \psi_1(z) &= c_{1,0} + c_{1,1}\cosh\lambda z\sin\lambda z + c_{1,2}\sinh\lambda z\cos\lambda z + c_{1,3}\cosh\lambda z\cos\lambda z + c_{1,4}\sinh\lambda z\sin\lambda z \\ &\quad + a_1\lambda z\cosh\lambda z\cos\lambda z + a_2\lambda z\sinh\lambda z\sin\lambda z + a_3(\sinh 2\lambda z - \sin 2\lambda z), \\ p_1 &= (24L\lambda^2\cosh 4\lambda a_3 + 16\lambda\sinh 4\lambda a_3 + 2L\lambda\cosh 2\lambda p_0^2 + \sinh 2\lambda p_0^2 + 4L\lambda^3\cosh 4\lambda c_{0,1}^2 \\ &\quad + 2\lambda^2\sinh 4\lambda c_{0,1}^2 + 4L\lambda^3\cosh 4\lambda c_{0,2}^2 + 2\lambda^2\sinh 4\lambda c_{0,2}^2 + 2\lambda\cos\lambda(2(4(2+L)\lambda\cosh\lambda \\ &\quad - 2L\lambda\cosh 3\lambda + 2\sinh\lambda + 8L\lambda^2\sinh\lambda - \sinh 3\lambda)a_1 + 2(2\sinh\lambda + 4L\lambda(\cosh 3\lambda - 2\lambda\sinh\lambda) \\ &\quad + 3\sinh 3\lambda)a_2 + p_0(-(2L\lambda\cosh 3\lambda + 2\sinh\lambda] + \sinh 3\lambda)c_{0,1} + (2L\lambda\cosh 3\lambda + \sinh 3\lambda)c_{0,2})) \\ &\quad - 4L\lambda^2\cos 4\lambda\left(6a_3 + \lambda(c_{0,1}^2 + c_{0,2}^2)\right) - 2\lambda\sin 4\lambda\left(8a_3 + \lambda(c_{0,1}^2 + c_{0,2}^2)\right) \\ &\quad + 2\lambda\sin\lambda(-2((-2 + 8L\lambda^2)\cosh\lambda + 3\cosh 3\lambda + 4L\lambda\sinh 3\lambda)a_1 \\ &\quad - 2((2 + 8L\lambda^2)\cosh\lambda + \cosh 3\lambda + 4(2+L)\lambda\sinh\lambda + 2L\lambda\sinh 3\lambda)a_2 \end{aligned}$$

$$
\begin{aligned}
&+p_0(-2\cosh\lambda c_{0,2}+(\cosh 3\lambda+2L\lambda\sinh 3\lambda)(c_{0,1}+c_{0,2})))\\
&+2\lambda\cos 3\lambda(-2L\lambda\cosh\lambda(2a_1+4a_2+p_0(-c_{0,1}+c_{0,2}))\\
&+\sinh\lambda(-6a_1+2a_2+p_0(c_{0,1}+c_{0,2})))-2\lambda\sin 3\lambda(\cosh\lambda(2a_1+6a_2+p_0(-c_{0,1}+c_{0,2}))\\
&+2L\lambda\sinh\lambda(-4a_1+2a_2+p_0(c_{0,1}+c_{0,2})))\\
&-\sin 2\lambda\left(96L\lambda^2\sinh 2\lambda a_3+p_0^2+4\lambda\cosh 2\lambda\left(16a_3+\lambda\left(c_{0,1}^2+c_{0,2}^2\right)\right)\right)\\
&+2\lambda\cos 2\lambda\left(-Lp_0^2+2\sinh 2\lambda\left(16a_3+\lambda\left(c_{0,1}^2+c_{0,2}^2\right)\right)\right)\Big)\\
&\Big/(8(2L\lambda\cos 2\lambda-2L\lambda\cosh 2\lambda+\sin 2\lambda-\sinh 2\lambda)),
\end{aligned}
$$

$$
v_1(z)=\frac{-2\lambda^2p_1-\lambda^2v_0^2(z)-\lambda^2\psi_0{}'2(z)-\psi_1{}'t'(z)}{2\lambda^2},
$$

$$
\begin{aligned}
\Theta_1(z)=\frac{1}{2}(1-z^2+Pr\lambda(&-\cos\lambda\cosh\lambda c_{0,1}+\cos z\lambda\cosh z\lambda c_{0,1}+\sin\lambda\sinh\lambda c_{0,1}\\
&-\sin z\lambda\sinh z\lambda c_{0,1}+\cos\lambda\cosh\lambda c_{0,2}-\cos z\lambda\cosh z\lambda c_{0,2}+\sin\lambda\sinh\lambda c_{0,2}\\
&-\sin z\lambda\sinh z\lambda c_{0,2}+z\cosh\lambda\sin\lambda c_{0,3}-\cosh z\lambda\sin z\lambda c_{0,3}+z\cos\lambda\sinh\lambda c_{0,3}\\
&-\cos z\lambda\sinh z\lambda c_{0,3}+z\cosh\lambda\sin\lambda c_{0,4}-\cosh z\lambda\sin z\lambda c_{0,4}-z\cos\lambda\sinh\lambda c_{0,4}\\
&+\cos z\lambda\sinh z\lambda c_{0,4})),
\end{aligned}
\qquad (17)
$$

where

$$
\begin{aligned}
c_{1,0}&=0,\\
c_{1,1}&=(\cos\lambda(4L\lambda\sin\lambda(\lambda-\cosh\lambda\sinh\lambda)+\cos\lambda(-2(1+L)\lambda+2L\lambda\cosh 2\lambda+\sinh 2\lambda))a_1\\
&\quad+\sinh\lambda(4L\lambda\cosh\lambda(\lambda+\cos\lambda\sin\lambda)+(2\lambda(1+L+L\cos 2\lambda)+\sin 2\lambda)\sinh\lambda)a_2\\
&\quad+(\cos 3\lambda(2L\lambda\cosh\lambda-\sinh\lambda)+\sin 3\lambda(\cosh\lambda+4L\lambda\sinh\lambda)\\
&\quad+\cos\lambda(-6L\lambda\cosh\lambda+4L\lambda\cosh 3\lambda-6\sinh\lambda+\sinh 3\lambda)\\
&\quad+\sin\lambda(\cosh 3\lambda+2L\lambda(3\sinh\lambda+\sinh 3\lambda)))a_3)\\
&\quad/(2L\lambda\cos 2\lambda-2L\lambda\cosh 2\lambda+\sin 2\lambda-\sinh 2\lambda),\\
c_{1,2}&=(\cosh\lambda(-\cosh\lambda(-2(1+L)\lambda+2L\lambda\cos 2\lambda+\sin 2\lambda)+4L\lambda(\lambda-\cos\lambda\sin\lambda)\sinh\lambda)a_1\\
&\quad-\sin\lambda(4L\lambda\cos\lambda(\lambda+\cosh\lambda\sinh\lambda)+\sin\lambda(2\lambda(1+L+L\cosh 2\lambda)+\sinh 2\lambda))a_2\\
&\quad+(\cos 3\lambda(4L\lambda\cosh\lambda+\sinh\lambda)+\sin 3\lambda(\cosh\lambda-2L\lambda\sinh\lambda)\\
&\quad+\cos\lambda(2L\lambda(-3\cosh\lambda+\cosh 3\lambda)+\sinh 3\lambda)\\
&\quad-\sin\lambda(6\cosh\lambda+\cosh 3\lambda+6L\lambda\sinh\lambda+4L\lambda\sinh 3\lambda))a_3)\\
&\quad/(2L\lambda\cos 2\lambda-2L\lambda\cosh 2\lambda+\sin 2\lambda-\sinh 2\lambda),\\
c_{1,3}&=0,\\
c_{1,4}&=0,\\
a_1&=\frac{1}{8}p_0(c_{0,1}+c_{0,2}),\\
a_2&=\frac{1}{8}p_0(c_{0,1}-c_{0,2}),\\
a_3&=-\frac{1}{10}\lambda(c_{0,1}^2+c_{0,2}^2).
\end{aligned}
\qquad (18)
$$

Table 1. Quantitative comparisons with data in Batista (2011) within parenthesis

n	u_{max}	z_{max}	$-v_{min}$	z_{min}
1	197.279 (197.2)	0.962828 (0.9628)	652.923 (652.9)	0.888485 (0.8885)
2	185.903 (185.9)	0.960532 (0.9605)	690.414 (690.4)	0.883208 (0.8832)
3	184.356 (184.4)	0.960618 (0.9606)	707.791 (707.8)	0.881751 (0.8818)

Source: Author's own work

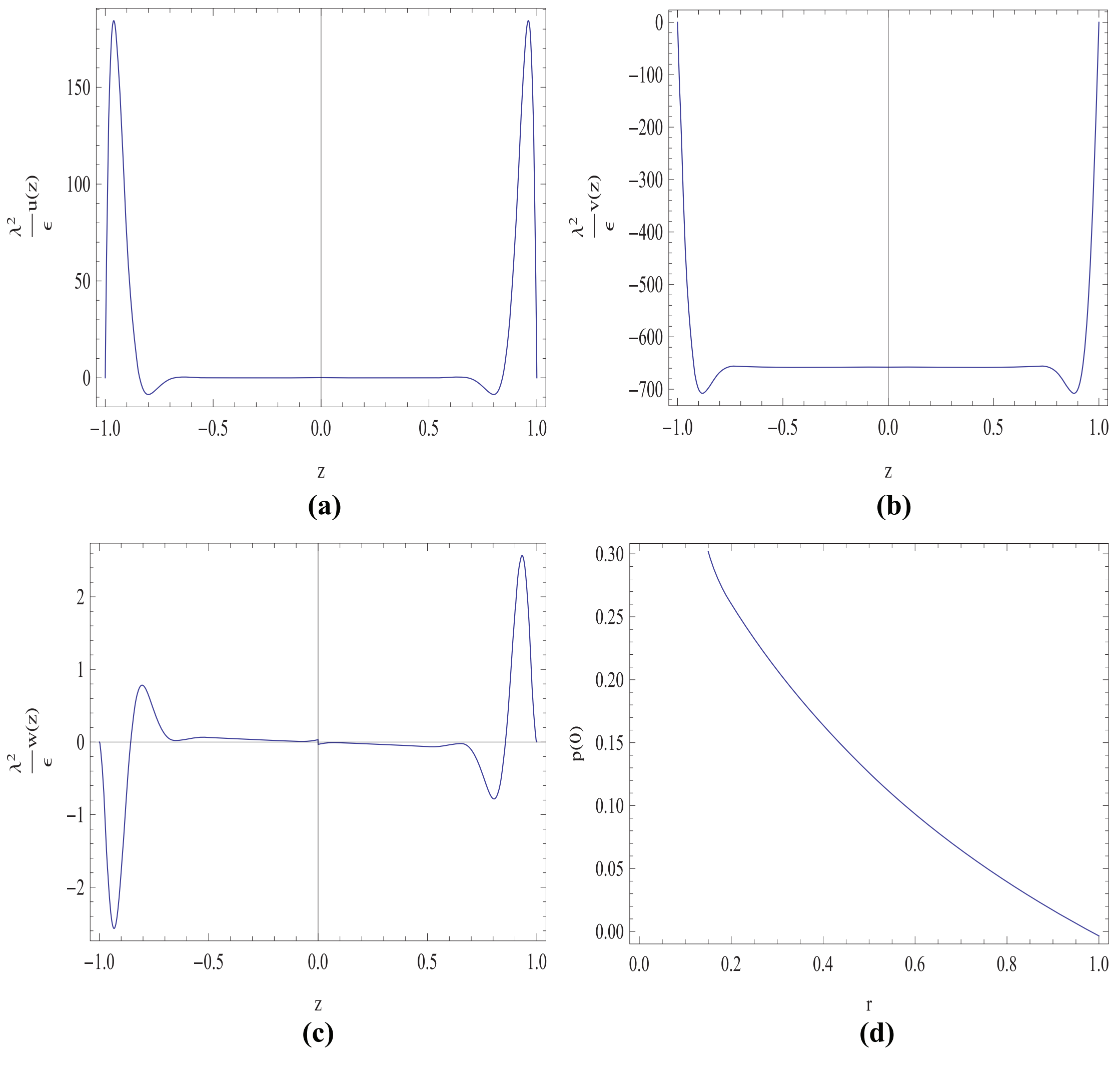

Source: Author's own work

Figure 2. (a) Radial flow u, (b) circumferential flow v, (c) axial flow w and (d) pressure distribution at the centerline $p(0)$

Although not given here due to its lengthy expressions, the next-order term $\Theta_2(z)$ was also calculated analytically and used in the series form in equation (10) in further computations.

The third-order solutions are cumbersome and naturally complex to evaluate analytically. Therefore, they are obtained by solving the corresponding third-order equations numerically from the system (13)–(14) setting $n = 0$. Such a procedure is obligatory, as also highlighted in the no-slip fluid flow research in Batista (2011).

4. Results and discussion

To justify the foregoing analytical perturbation results, we initially made a raw comparison with the experimental input list $C_w = 100$, $\lambda = 21.1289$, $\epsilon = 0.133665$ and $r = 0.54955$ given in Batista (2011) for the special case of no-slip. We should note, as aforementioned, that only the third-order approximations are treated numerically, with analytical expressions for the

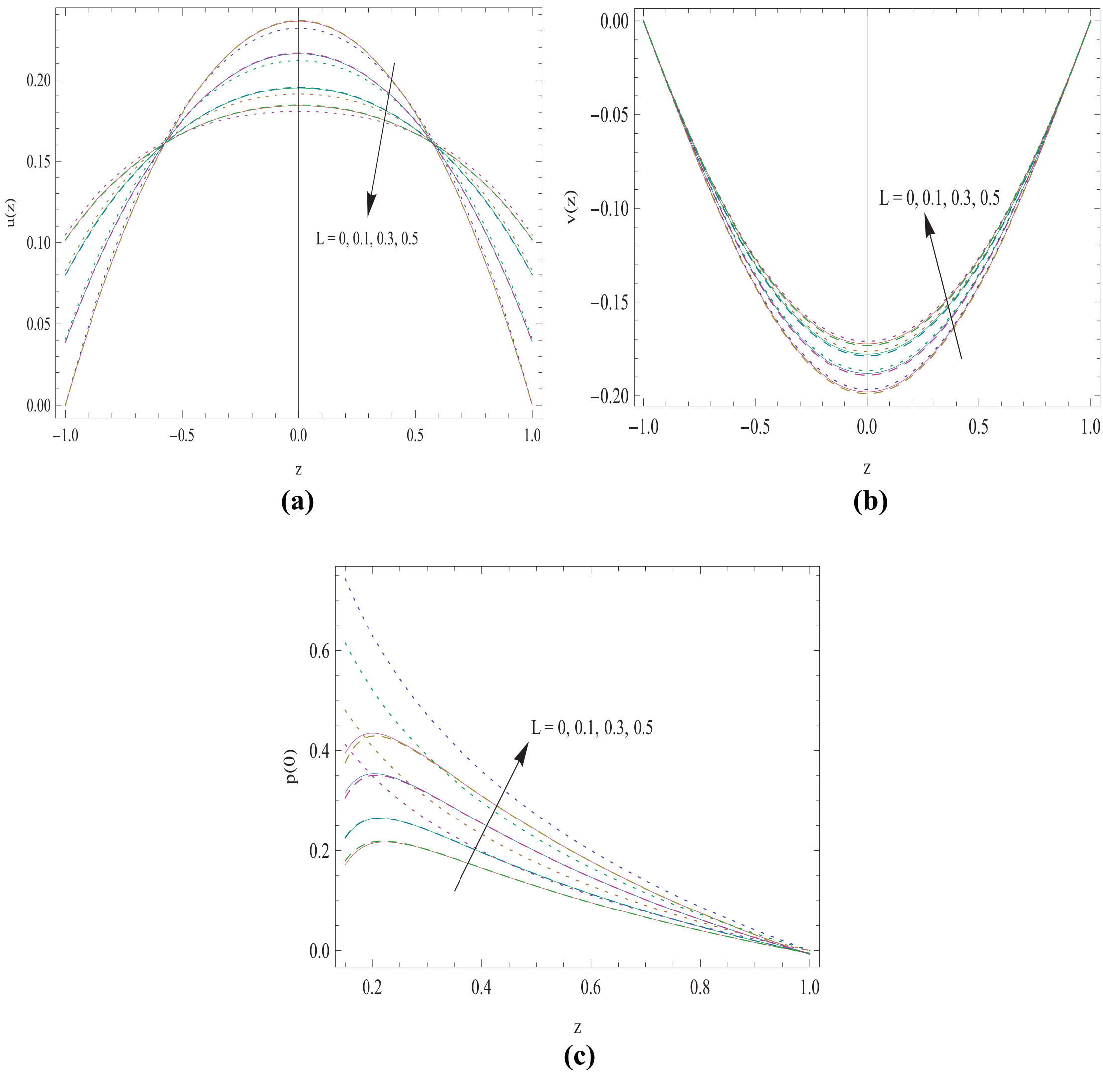

Source: Author's own work

Figure 3. $\lambda = 1$. (a) Radial flow u, (b) circumferential flow v and (c) pressure distribution at the centerline $p(0)$. For style of the curves, please refer to the text

first and second orders. The accuracy of such an approach was also verified in Batista (2011). Table 1 is to provide a reinforcement of the accuracy of present work. When compared to Figures 2–5 presented in Batista (2011), Figure 2(a)–(d) and Table 1 exhibit excellent qualitative and quantitative agreements. It is noticed that the scaling in velocity components was adopted to comply with the quantities in Batista (2011), which in turn complies with the results of Crespo del Arco *et al.* (1996), too.

To assure the convergence of the series in equation (10) for the parameter range studied within the present research, we next demonstrate a sample in Figure 3(a)–(c) incorporating the impacts of slip for the chosen parameters $\epsilon = 0.1$, $r = 0.5$, $\lambda = 1$ and $C_w = 10$. Up to third-order truncation is permitted again in the perturbation series. Precisely, the dotted curves correspond to the first-order solutions, while the unbroken curves to the second-order and the dashed curves to the third-order solutions. Such a

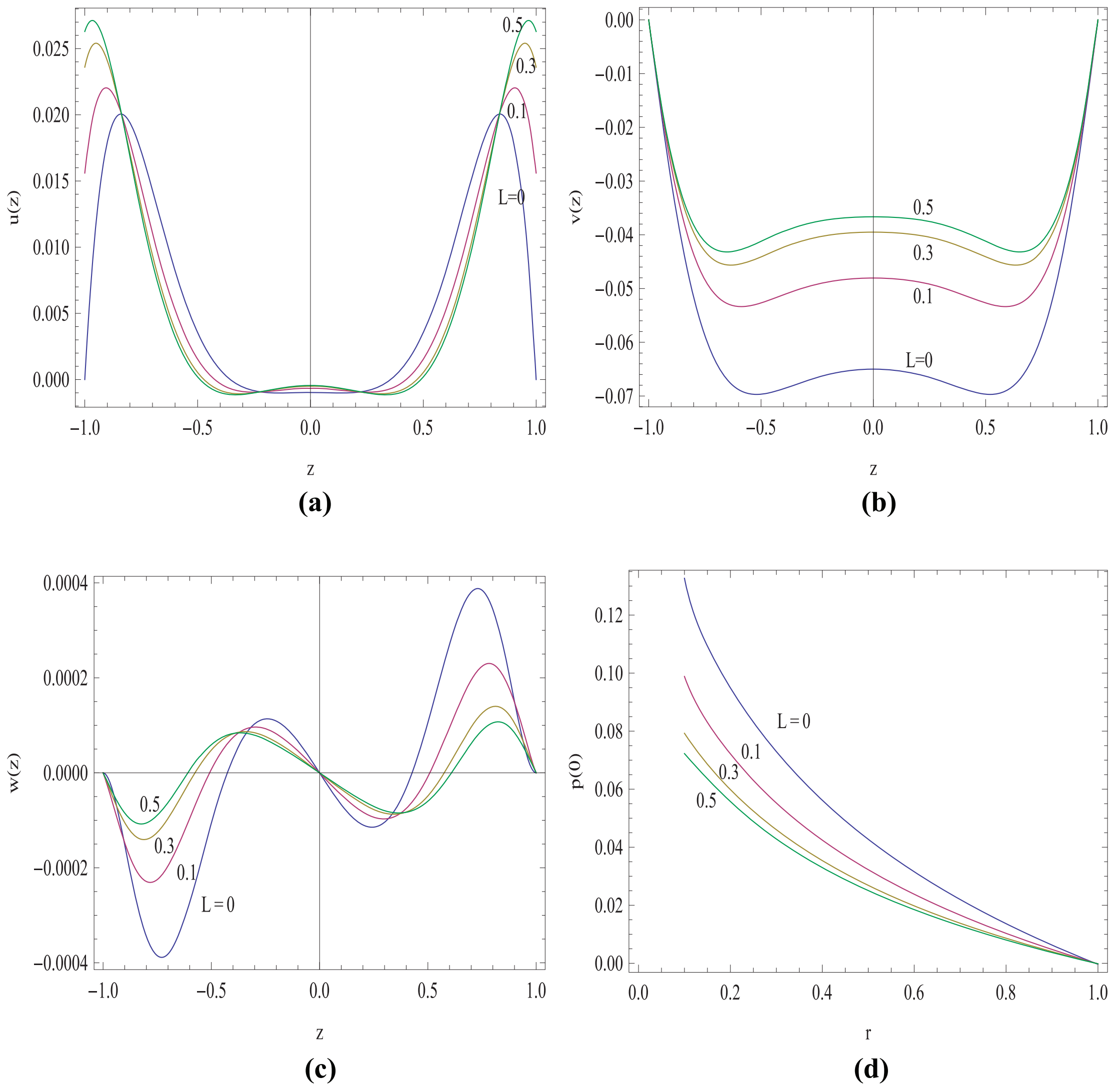

Source: Author’s own work

Figure 4. $\lambda = 5$. (a) Radial flow u, (b) circumferential flow v, (c) axial flow w and (d) pressure distribution at the centerline $p(0)$

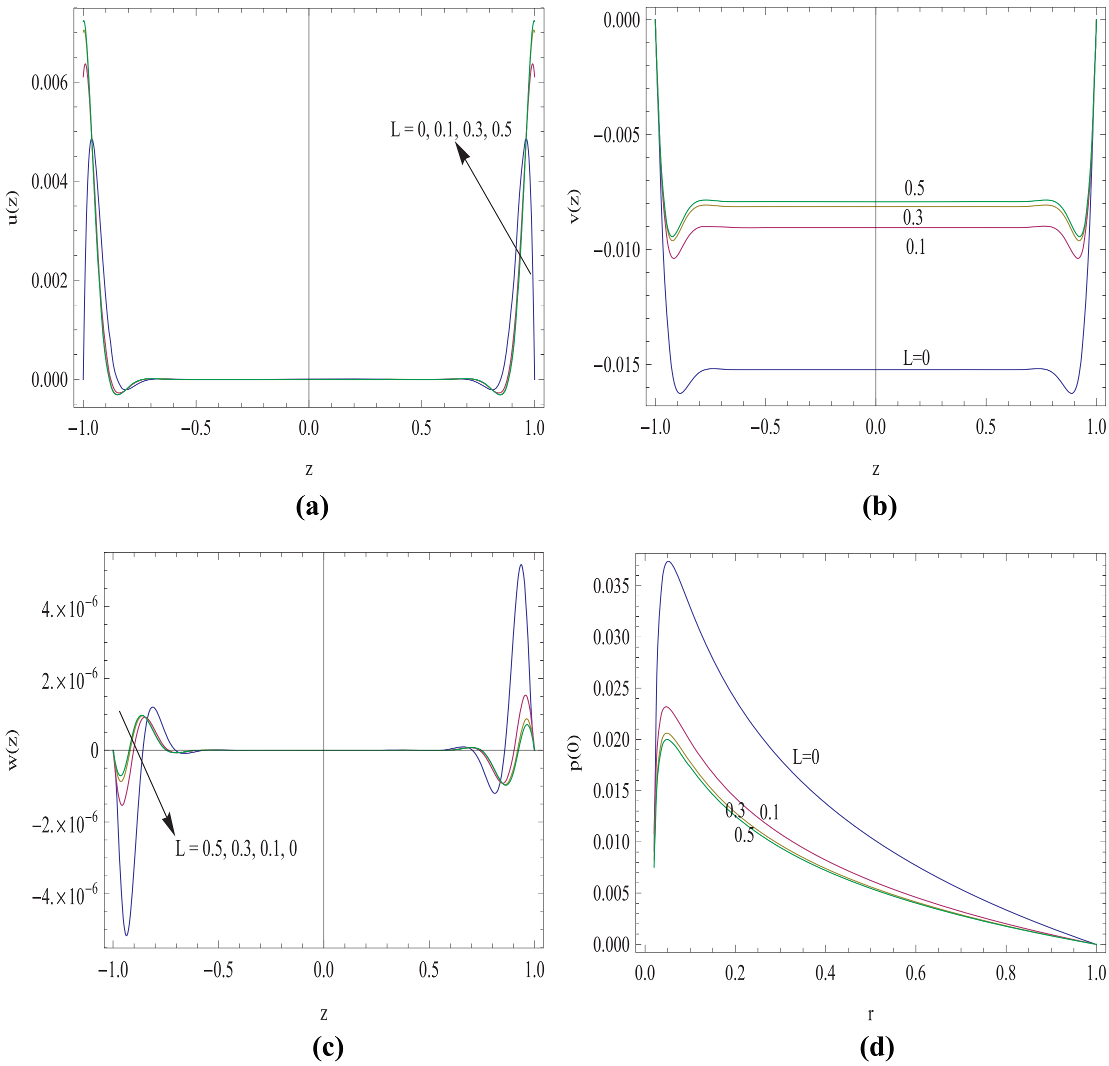

Source: Author's own work

Figure 5. $\lambda = 21$. (a) Radial flow u, (b) circumferential flow v, (c) axial flow w and (d) pressure distribution at the centerline $p(0)$

laminar flow regime pertinent to small Reynolds numbers with parabolic velocity profiles was also recently visualized experimentally in Schosser *et al.* (2019) under no-slip assumption. The second and third order flow contributions are indicating a clear and plausible convergence, whereas the convergence is roughly confined to the domain between the inlet and outlet radial locations $r \in [0.2, 1]$ for small slip parameters, as clear from the midway pressure distribution in Figure 3(c). The effects of slip on the radial and tangential velocity components in Figure 3(a) and (b), are to reduce the maximum velocities and to flatten the radial velocity profile. The actual peripheral velocity component should be assessed by further adding $\epsilon r = 0.05$ to $v(z)$ shown in Figure 3(b). Hence, the fluid revolving with the disk system close to the disk surface starts revolving in the opposite direction as the midway is approached. Another insight to gain is that the range of applicability of the series solution (10) in the radial coordinate gets enhanced as more effective slip is taken into account, see Figure 3(c). The actual pressure should be considered by adding the extra term $\frac{1}{2}\epsilon^2 r^2$ to the calculated p in the figure.

The velocity and pressure profiles from the second-order series truncation in equation (10) in the creeping flow limit yield the following polynomial solutions:

$$
\begin{aligned}
\frac{\lambda^2}{\epsilon}u(z) &= 3C_w\oint\Big(560\pi(r+3Lr)^2(1+2L-z^2) \\
&\quad + C_w(5+45L+98L^2-3(11+7L(11+20L))z^2+35(1+L(5+6L))z^4-7(1+3L)z^6)\epsilon) \\
&\quad \Big/\Big(4480\pi^2(r+3Lr)^3\Big), \\
\frac{\lambda^2}{\epsilon}v(z) &= 0, \\
\frac{\lambda^2}{\epsilon}w(z) &= -\frac{3C_w^2 z(-1+z^2)(5+45L+98L^2-2(1+3L)(3+7L)z^2+(1+3L)z^4)\epsilon}{2240(1+3L)^3\pi^2 r^4}, \\
\lambda^4 p(z) &= \frac{3C_w\epsilon\Big(-9C_w(2+7L(2+5L(1+L)))\epsilon-280\pi(r+3Lr)^2\ln r\Big)}{1120(1+3L)^3\pi^2 r^2}.
\end{aligned}
\tag{19}
$$

In addition, when L is set to zero, equation (19) leads to the no-slip solutions:

$$
\begin{aligned}
\frac{\lambda^2}{\epsilon}u(z) &= -\frac{3C_w(-1+z^2)(560\pi r^2+C_w(5-28z^2+7z^4)\epsilon)}{4480\pi^2 r^3}, \\
\frac{\lambda^2}{\epsilon}v(z) &= 0, \\
\frac{\lambda^2}{\epsilon}w(z) &= -\frac{3C_w^2 z(-5+z^2)(-1+z^2)^2\epsilon}{2240\pi^2 r^4}, \\
\lambda^4 p(z) &= -\frac{3C_w\epsilon(9C_w\epsilon+140\pi r^2 \ln r)}{560\pi^2 r^2},
\end{aligned}
\tag{20}
$$

that perfectly agree with those expressions given in Sengupta and Guha (2012) and Beans (1966). Notice that parabolic channel flow is achieved when further the thickness $\epsilon \longrightarrow 0$ to give:

$$
\frac{\lambda^2}{\epsilon}u(z) = \frac{3C_w(1+2L-z^2)}{8\pi r(1+3L)}, \tag{21}
$$

refer to the solution in Schosser *et al.* (2019) for the no-slip case.

Having confidence in the accuracy and convergence of the perturbation series solutions (10), we can carry on now investigating effects of combinations of physical parameters on the flow, pressure and temperature fields with the third level truncation in the series (10) for the range of parameters studied here. It should be recalled that the number of terms in the series may need to be increased further for the convergence for other set of parameters (particularly as the inlet location is very small), which is beyond the scope of the present analysis. Figure 4(a)–(d) exhibit the velocity and pressure distributions for the parameters

$\epsilon = 0.1$, $r = 0.5$, $\lambda = 5$ and $C_w = 10$. As compared to the low Reynolds number flow regime in Figure 3(a)–(c), the parabolic shape deforms considerably, and the radial and circumferential flow develop mainly adjacent to the disk surfaces. The middle region of the disk almost settles down. The axial velocity component has smaller magnitude as compared to the others. Slip strictly suppresses the momentum layer, apart from the disk surface region where the slip is applied, as physically expected. Besides the acceleration influence of the slip for the radial velocity of the fluid particles next to the wall, it also changes the direction of angular rotation completely, as clarified in Figure 4(b), after adding the quantity 0.05 to $v(z)$. The reduction in pressure with larger slips leads to less axial velocity of fluid particles. Also, to conserve the mass balance, the fluid particles drawn toward the disk surfaces are driven radially outwards.

Figure 5(a)–(d) reveal a higher Reynolds number together with the slip effects at $\lambda = 21$ ($Re = \lambda^2$). A viscous boundary layer inevitably forms next to the disk walls, in parallel to the

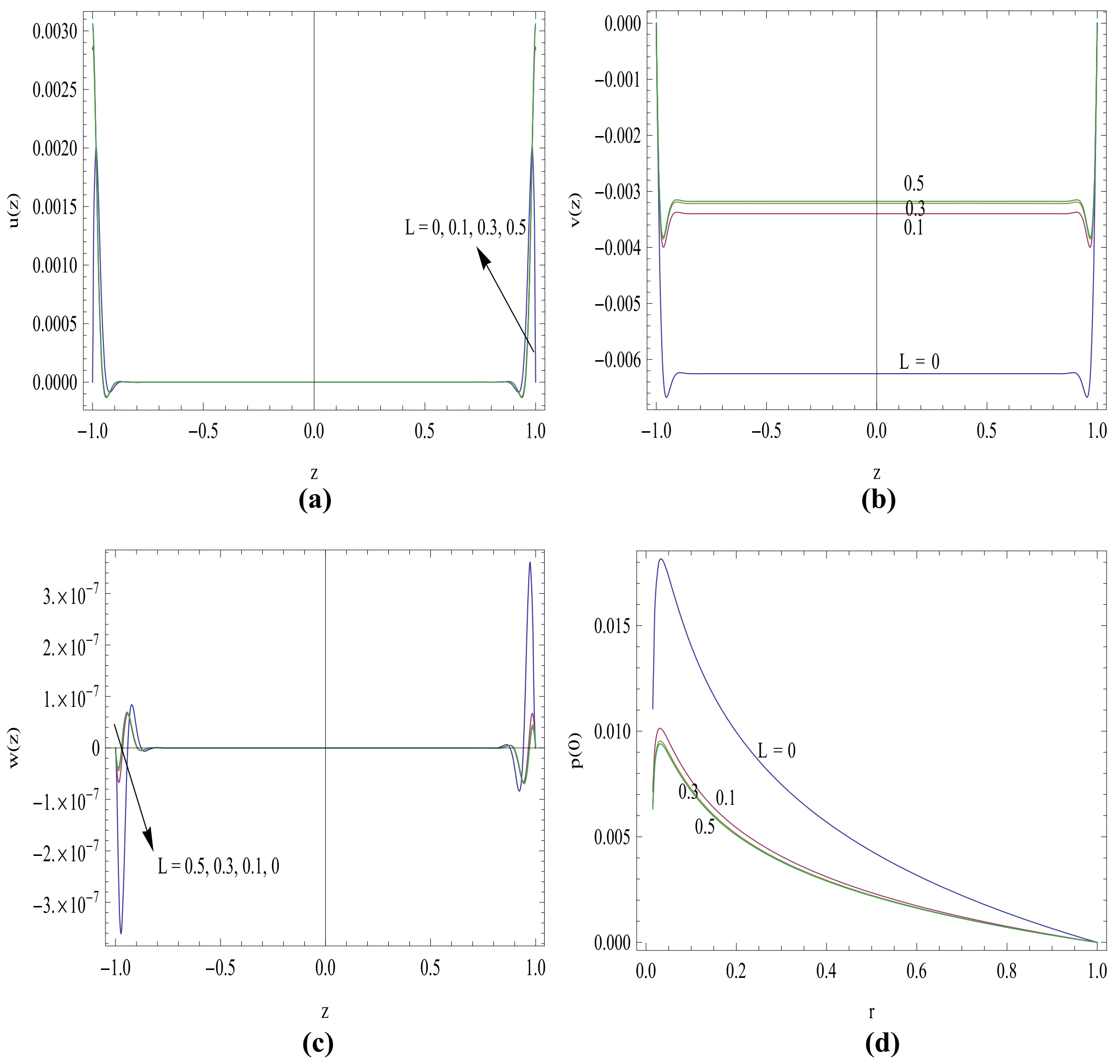

Source: Author's own work

Figure 6. $\lambda = 51$. (a) Radial flow u, (b) circumferential flow v, (c) axial flow w and (d) pressure distribution at the centerline $p(0)$

physical expectation. Increase in the Reynolds number and the slip let the tangential fluid velocity tend to the rotational speed of the disk surface, hence almost a rigid-body rotation is observed. The viscous pumping action confines the flow phenomenon to the vicinity of the disks and by decreasing the flow and pressure quantities, with more pronounced effect on the axial velocity of the fluid particles.

Figure 6(a)–(d) demonstrate the most thin viscous sublayer at the Reynolds number $Re = \lambda^2 = 51^2$. We should note that at this high Reynolds number the flow may have already gone into the turbulent stage (subject to the experimental verification), and these solutions are then questionable, only capturing a qualitative representation. Absolute/convective type instabilities may then dominate the system, see Viaud *et al.* (2008).

The influences of slip parameter on the radial wall velocity $u(-1)$ and wall shear rate $u'(-1)$ are afterwards anticipated in Figure 7 at the parameters of Batista (2011). The slip absolutely increases the wall velocities of the particles, and it yields a reduction in the wall shear. This outcome is also in line with the results of slip on the laminar jet flow Turkyilmazoglu (2019).

As for the effects of slip/no-slip on the thermal layer, the creeping flow thermal limit gives rise to the second-order approximation:

$$\begin{aligned}\Theta(z) = \Big(&C_w^2\mathrm{Pr}(-1+z^2)(-38-4533\mathrm{Pr}-L(418+34935\mathrm{Pr}+504L(2+3(59+50L)\mathrm{Pr}))\\&+82z^2+\big(2L(331+672L)+3(1+3L)(589+112L(19+15L))\mathrm{Pr}\big)z^2\\&-(1+3L)(50+543\mathrm{Pr}+56L(2+21\mathrm{Pr}))z^4+3(1+3L)(2+15\mathrm{Pr})z^6\Big)\epsilon^2\end{aligned}$$

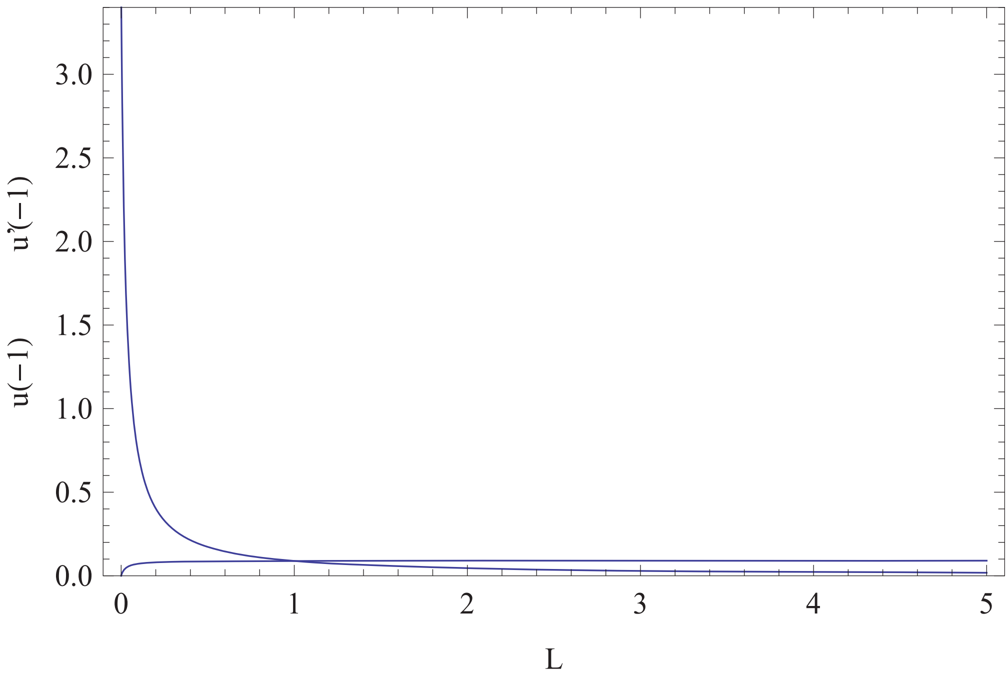

Source: Author's own work

Figure 7. Wall velocity and shear stress for the data of Batista (2011).

$$+224C_w(1+3L)^2\pi\mathrm{Pr}(-1+z^2)\epsilon(10r^2(-5-12L+z^2)$$
$$+3(-83+22z^2-3z^4+40L(-5+z^2))\epsilon^2)$$
$$+8960(1+3L)^3\pi^2(8r^4-4r^2(-1+z^2)\epsilon^2$$
$$+3(5-6z^2+z^4)\epsilon^4))/71680(1+3L)^3\pi^2r^4, \tag{22}$$

and further $L\rightarrow 0$ yields:

$$\begin{aligned}\Theta(z) = \Big(&C_w^2\mathrm{Pr}(-1+z^2)(-38-4533\mathrm{Pr}+(82+1767\mathrm{Pr})z^2-(50+543\mathrm{Pr})z^4\\ &+3(2+15\mathrm{Pr})z^6)\epsilon^2+224C_w\pi\mathrm{Pr}(-1+z^2)\epsilon(10r^2(-5+z^2)\\ &-3(83-22z^2+3z^4)\epsilon^2)+8960\pi^2(8r^4-4r^2(-1+z^2)\epsilon^2\\ &+3(5-6z^2+z^4)\epsilon^4)\Big)\Big/71680\pi^2r^4.\end{aligned} \tag{23}$$

The natural temperature solution of unity will appear if further the gap thickness tends to zero.

Thermal fields are seen in Figures 8(a), (b) and 9(a), (b) for the selected physical parameters. Temperature profiles are parabolic regardless of the slip and Reynolds number, though the shape is slightly affected adjacent to the walls. As a consequence, the particles are carried through the tube at a higher temperature away from the disk surface. Reduction impact of slip on the momentum layer has also the similar influence on the temperature field, with a lesser order of magnitude though.

Eventually, the centerline temperature $\Theta(0)$ and wall temperature gradient $\Theta'(-1)$ are shown in Figure 10(a) and (b), for $\epsilon = 0.1$, $r = 0.5$, $C_w = 1$ and $Pr = 1$, with varying λ against

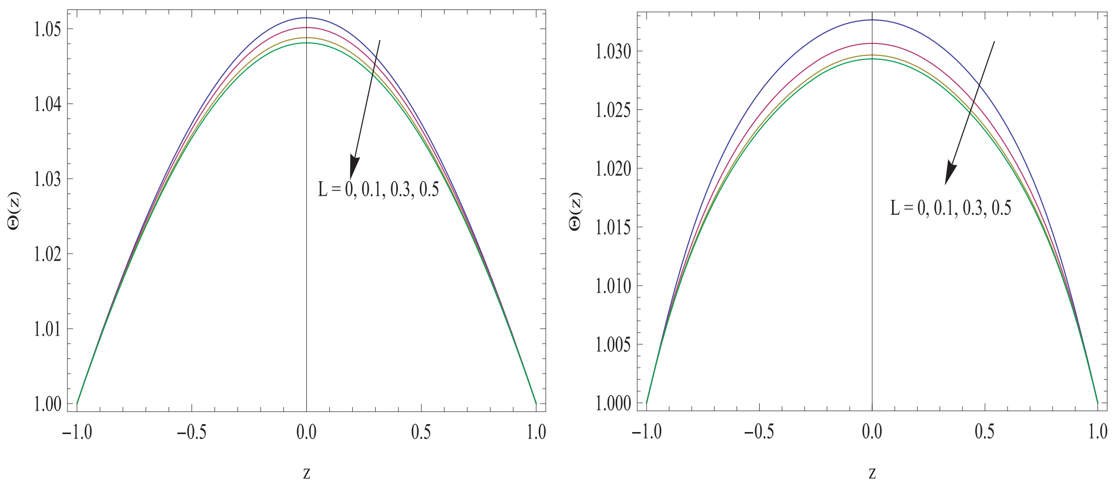

(a) **(b)**

Notes: (a) $\lambda = 1$; (b) $\lambda = 5$
Source: Author's own work

Figure 8. Temperature field for $\epsilon = 0.1$, $r = 0.5$, $C_w = 1$ and $Pr = 1$

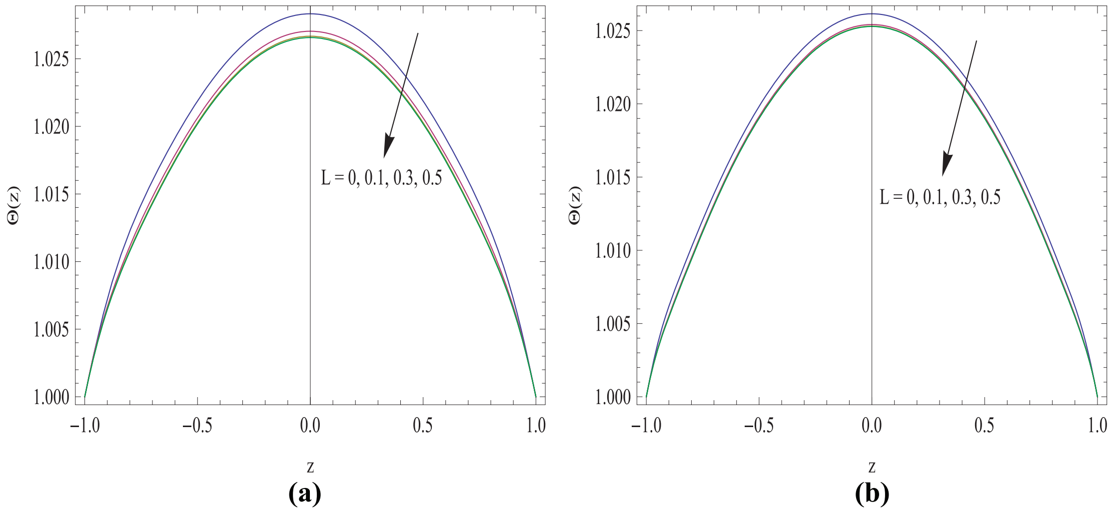

Notes: (a) $\lambda = 10$; (b) $\lambda = 21$
Source: Author's own work

Figure 9. Temperature field for $\epsilon = 0.1$, $r = 0.5$, $C_w = 1$ and $Pr = 1$

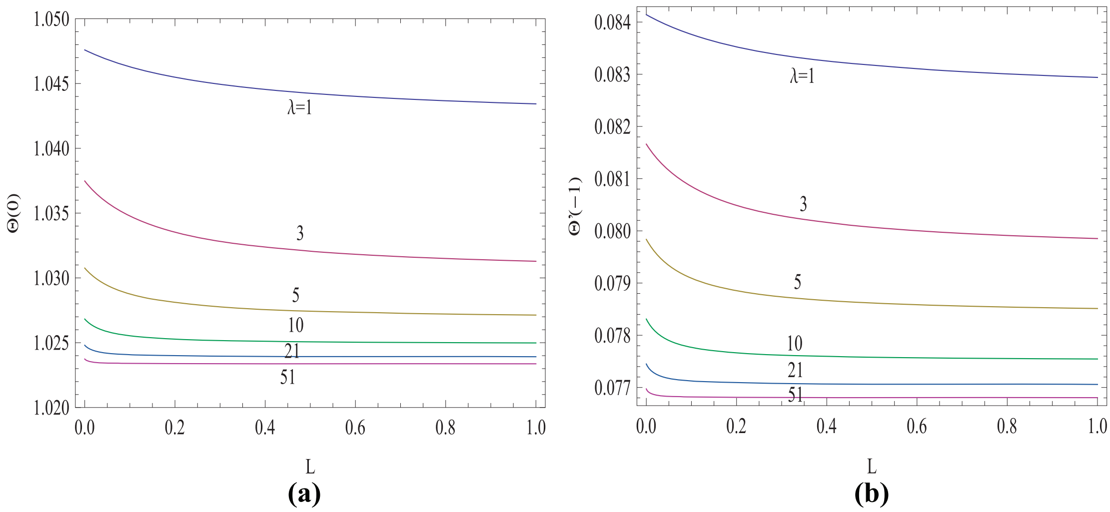

Notes: (a) Centerline temperature; (b) wall temperature gradient
Source: Author's own work

Figure 10. Temperature field for $\epsilon = 0.1$, $r = 0.5$, $C_w = 1$ and $Pr = 1$

L. The results are in parallel to those shown in the previous figures. Intriguingly, heat transfer from the surface is reduced both as λ and L are increased, overlapping with the findings in Kim *et al.* (1994). This is as a result of fluid getting cooled down within the disks by the action of these parameters, refer also to Turkyilmazoglu (2019) for a similar outcome on the slip wall jet.

5. Conclusions

This study uses an analytical approach to examine the impact of radial velocity slip on the flow and temperature field of an incompressible, viscous fluid flowing between parallel,